JOURNAL OF MATERIALS SCIENCE 25 (1990) 4427–4439

Microstructure and fracture behaviour of short and long fibre-reinforced polypropylene composites

D. E. SPAHR*, K. FRIEDRICH†
Polymer and Composites Group, Technical University Hamburg-Harburg, 2100 Hamburg 90, FRG

J. M. SCHULTZ
Department of Chemical Engineering, University of Delaware, Newark, Delaware 19716, USA

R. S. BAILEY
Advanced Materials Group, Imperial Chemical Industries, Wilton Centre, Cleveland TS6 6JE, UK

Microstructure and fracture mechanical behaviour of injection-moulded, longer glass fibre-reinforced polypropylene (Verton®; aspect ratio $\approx$ 320) were studied as a function of fibre volume fraction and compared to that of shorter fibre-filled polypropylene (aspect ratio $\approx$ 70). Toughness was measured using instrumented notched Izod and falling weight impact tests, as well as compact tension specimens. It was found that the addition of longer fibres generally increased the toughness of the material, although more significant increases were seen in the impact tests than were seen in the compact tension test. For the latter results, a correlation between toughness improvement and microstructural details was performed on the basis of the microstructural efficiency concept, a semi-empirical approach of the form $K_{c,C} = (a^* + nR)K_{c,M}$, where, $K_{c,C}$ and $K_{c,M}$ are the fracture toughnesses of the composite and the matrix, respectively, a^* is a matrix stress correction factor, n is a scaling parameter and R is a fibre reinforcement effectiveness factor. The latter corrects for differences in the composite microstructures, and incorporates effective fibre orientation factors, layering of injection moulded parts, and fibre volumes in the different layers.

Nomenclature

a	crack length
a^*	matrix toughness correction factor
A	cross-sectional area
B	thickness of the sample plaques
C	thickness of the composite core regions
E_{peak}	energy adsorbed up to the maximum force in the impact load–displacement curve
E_t	tensile modulus
F_{max}	maximum force in impact force–displacement curves
f_p	fibre orientation factor
f_{pe}	effective orientation factor
$f_{pe,C}$	effective orientation parameter, core region
$f_{pe,S}$	effective orientation parameter, surface region
F	critical load in the tensile test load–displacement curves
K_C	critical stress intensity factor/fracture toughness
K_L	fracture toughness of the composite materials
K_d	dynamic fracture toughness
K_L	fracture toughness of the matrix
L	test with crack parallel to the mould filling direction
M	microstructural efficiency factor
n	scaling parameter for reinforcement effectiveness factor (energy absorbtion ratio)
R	reinforcement effectiveness factor
S	thickness of the composite surface regions
T	test with crack perpendicular to the mould filling direction
V_f	fibre volume fraction
V_m	matrix volume fraction $(= 1 - V_f)$
W	specimen width
w_f	fibre weight fraction
w_m	matrix weight fraction $(= 1 - w_f)$
X_n	number average fibre length
X_v	volume average fibre length
$Y(a/W)$	polynomial correction for compact tension specimens
α	variable in effective orientation factor formula
β	variable in effective orientation factor formula
ε_B	strain to break
ρ_c	density of the composite
ρ_f	fibre density
ρ_m	matrix density
σ_f	fracture strength
θ	fibre angle with respect to a reference direction

* *Present address:* Department of Chemical Engineering, University of Delaware, Newark, Delaware 19716, USA.
† *Present address*: Institute for Composite Materials, University of Kaiserslautern, 6750 Kaiserslautern, W. Germany.

0022–2461/90 $03.00 + .12

2. Introduction

It has recently become possible by a pultrusion compounding technique to produce injection-moulded polymer matrix composites with fibres whose aspect ratio ($\simeq 200$) greatly exceeds that of conventional fibre reinforced thermoplastic systems (≈ 20) [1]. The longer fibre reinforcement results in improved values of stiffness, strength and, in some cases, toughness and fatigue crack propagation resistance of this group of composites. This was clearly shown quite recently in studies performed on glass fibre/polyamide composites [2, 3].

The purpose of the studies presented in this paper was to examine the effects of longer glass fibre reinforcements on the fracture toughness of injection-moulded glass fibre/polypropylene composites. Several different testing geometries were used (compact tension, Izod impact, and falling weight impact), in order to compare the toughnesses found by these different methods. Especially interesting was a comparison of toughnesses which were essentially strength based (e.g. K_c from classical fracture mechanics) and the energy-related toughness values measured in impact tests.

3. Experimental procedure

3.1. Materials

Two sets of materials, all in the form of 160 mm × 160 mm plaques with a thickness of about $B = 3$ mm, were supplied by ICI, Wilton, UK; they were based on ICIs Verton® MFX 7008 (40% by weight glass fibre-reinforced coupled homopolymer polypropylene).

Set 1: neat polypropylene (PP) matrix, and PP filled with 10, 20, 30 and 40 wt % "longer" glass fibres (referred to as $10L_1$, $20L_1$, $30L_1$, $40L_1$, respectively), and 40 wt % "short" glass fibres ($40S_1$).

Set 2: polypropylene filled with 10, 20, 30 and 40 wt % "short" glass fibres (hereafter referred to as $10S_2$, $20S_2$, $30S_2$ and $40S_2$, respectively).

The long glass fibre materials were produced by the regular Verton® pultrusion technique, while the short glass fibre materials went through an extra extrusion process. All of the weight fractions are nominal. The values can be transferred into nominal fibre volume fraction by the following correlation

$$V_f = \frac{w_f/\rho_f}{w_f/\rho_f + w_m/\rho_m} \quad (1)$$

In reference to these samples, the x direction corresponds to the mould-filling direction (MFD), the y direction corresponds to the width and the z direction corresponds to the thickness. Mechanical test specimens had two different orientations. Samples whose cracks were parallel to the mould-filling direction are referred to as longitudinal (L) direction samples and samples whose cracks were perpendicular to the mould-filling direction are referred to as transverse (T) direction samples. The plaque geometry and sample orientations are shown schematically in Fig. 1.

3.2. Microstructural characterization

Studies on microstructural details of the different sets of materials were concentrated primarily on the

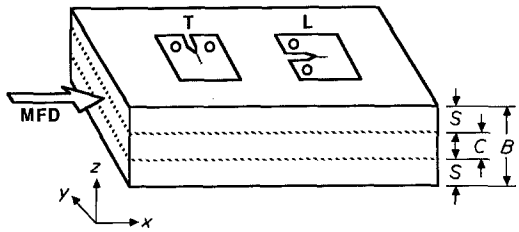

Figure 1 Macrostructure of injection-moulded plaques and orientation of the mechanical test specimens.

factors which resulted from the different amounts of fibre loading:

(a) the fibre volume fraction;

(b) the fibre orientation and its distribution across the plaque thickness B;

(c) the fibre length distribution.

Fibre orientation was measured on a variety of SEM or optical reflected-light micrographs taken from sections of the materials polished in the x–y planes. It was found that the fibres were primarily oriented in these planes, and that the fibres arranged themselves in a three-layer structure often found in injection-moulded fibre-filled materials [2, 4–9]. There were two surface layers (S) of fibres aligned primarily parallel to the mould filling direction (MFD) and a core region (C) of fibres aligned primarily perpendicular to the mould filling direction. This structure is shown in Fig. 2. The fibre orientation is expressed as a fibre orientation factor

$$f_p = 2\langle\cos^2\theta\rangle - 1 \quad (2)$$

where θ is the angle that the fibre makes with a reference direction and $\langle\cos^2\theta\rangle$ is the average of $\cos^2\theta$. The relative thickness of each layer was measured from scanning electron micrographs of the x–z and y–z planes (cf. Fig. 2).

For one part of the first set of long and short fibre-filled samples ($20L_1$, $40L_1$, $40S_1$), the distribution in fibre length was determined by burning off the

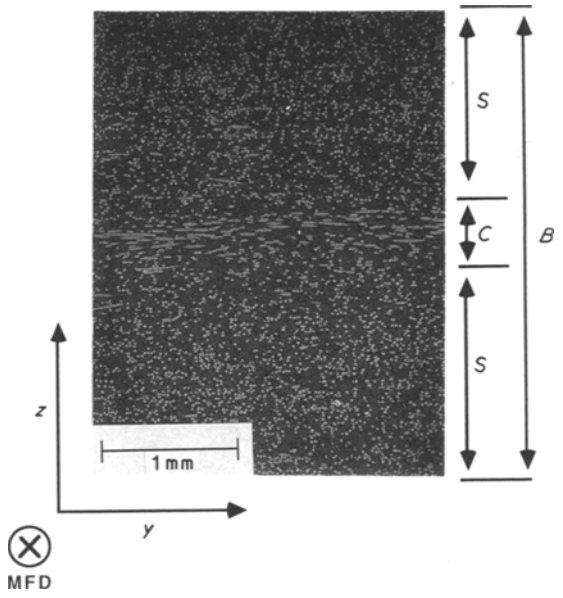

Figure 2 y–z plane of the $20L_1$ material showing a three-layer structure with the fibres in the surface (S) layer parallel to the MFD and the fibres in the core (C) perpendicular to the MFD.

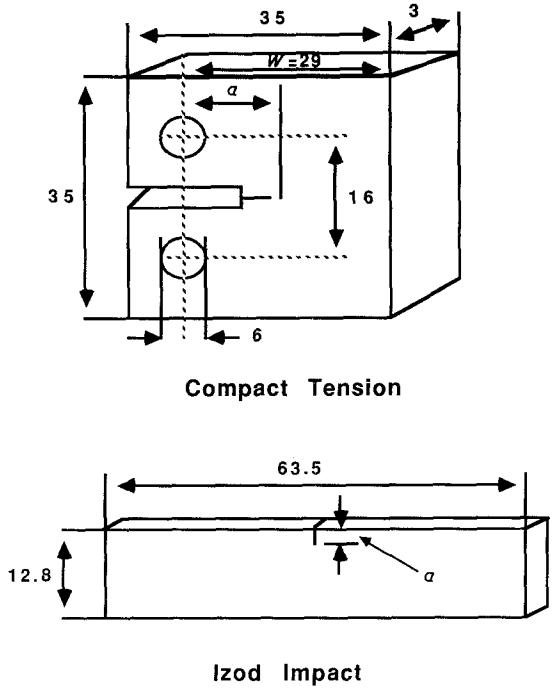

Figure 3 Geometry and dimensions of the mechanical test specimens.

matrix and then allowing the resultant fibres to settle on a stack of nine sieves (SV). Each layer was analysed separately this way. The fibre length distribution on each sieve was measured, whereby the data represent measurements on approximately 900 fibres.

For the second set of "short" fibre-reinforced systems ($10S_2$ to $40S_2$), fibre length measurements were carried out in a simpler way, i.e. by the use of light optical micrographs (LM) taken from the resultant fibres after burning off the polymer around them. To have a better basis for comparison, it was attempted to apply the same procedure to the first set of materials.

Density measurements were used to determine the overall fibre volume fractions of the different materials

$$\rho_c = \rho_f V_f + \rho_m V_m \quad (3)$$

In addition, the fibre volume fraction in each layer was measured by grinding samples to an appropriate thickness and then measuring the density of each section. The matrix was assumed to have the same density as the neat matrix (found to be $0.905\,g\,cm^{-3}$) throughout the thickness of the materials. This leads to a slight error, because it can be expected that the matrix should increase in crystallinity, and hence density, near the centre of the plaques. However, because the fibres are much denser than the matrix, the error should be small. The density of the fibres was assumed to be that of E-glass ($2.5\,g\,cm^{-3}$ [10]).

3.3. Fracture toughness measurements

Four kinds of mechanical tests were performed: (a) regular tensile tests with dog-bone-shaped specimens machined out of the injection-moulded plaques; (b) tensile tests on compact tension (CT) specimens (at a cross-head speed of $1\,mm\,min^{-1}$); (c) instrumented Izod impact tests (impact velocity of $3.5\,m\,sec^{-1}$); and (d) instrumented falling weight impact tests, using rectangular plaques, 50 mm × 50 mm in size (impact velocity of $6.3\,m\,sec^{-1}$ and a striker with a tip radius

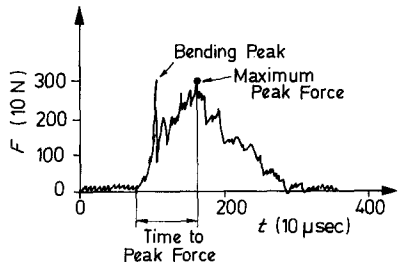

Figure 4 Typical instrumented impact force–time curve ($40L_1$ material, falling weight test).

of 20 mm). The compact tension specimens and the Izod specimens each had sharp cracks introduced with a razor blade. Fig. 3 shows their exact geometries. All tests were performed at room temperature. In addition, one CT-test series with the "longer" fibre-reinforced composites was carried out at 70° C.

Because the mechanical properties of these materials can be expected to be anisotropic, the tensile and Izod impact tests were measured in the two perpendicular directions (L and T), described above. The falling weight test has no orientation dependence, although the samples sometimes failed in an anisotropic manner.

Tensile fracture toughness values were calculated using the standard formula

$$K_c = \frac{F_c}{BWa^{1/2}} Y\left(\frac{a}{W}\right) \quad (4)$$

where F_c is the maximum load in the tensile load–displacement curve, and $Y(a/W)$ is the polynomial correction factor for compact tension specimens [11]. The instrumented impact tests give data in the form of force–time curves which can be integrated to give energy–time curves. Examples of these curves are shown in Figs 4 and 5. It is normally assumed that fracture begins at the time at which the force is a maximum. Both the energy adsorbed up to the beginning of fracture and the maximum force, which is a measure of the fracture strength of the material, will be reported.

4. Results and discussion

4.1. Microstructural features

A summary of various microstructural features measured is given in Table I. All of the composite specimens showed the three-layer structure mentioned

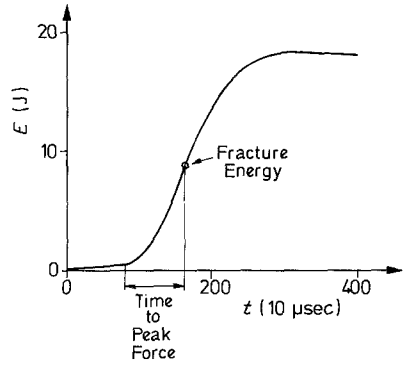

Figure 5 Typical instrumented impact energy–time curve ($40L_1$ material, falling weight test). Fracture time taken from Fig. 4.

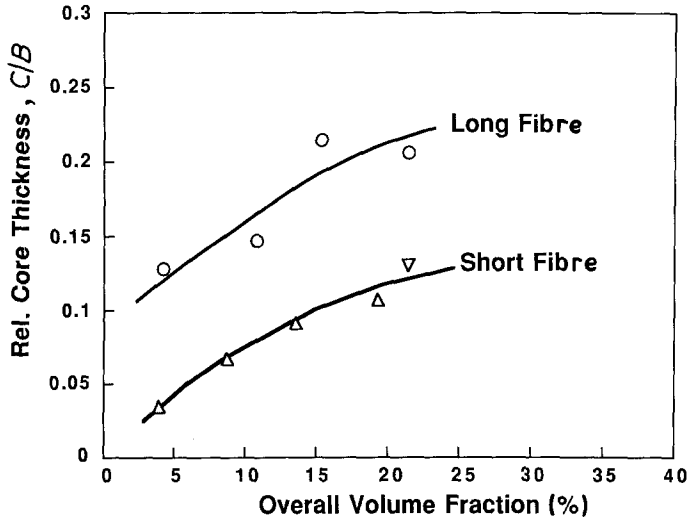

Figure 6 Change in core thickness with fibre volume fraction for long glass fibre (LGF)-PP and short glass fibre (SGF)-PP. (○) $10L_1$ to $40L_1$, (▽) $40S_1$, (△) $10S_2$ to $40S_2$.

above. It can be seen that the core thickness of both the short and the long fibre materials generally increased with volume fraction of fibres, although the $40L_1$ material had a core which was slightly thinner than the $30L_1$ material. Also, the short fibre materials had a considerably thinner core region than the long fibre material (Fig. 6). Further, it is shown in Table I that there exists a considerably higher concentration of fibres in the core region relative to the surface regions (Fig. 7).

Fibres in both the S and C layers of the materials became more highly oriented as the fibre volume fraction increased (Fig. 8). The $10L_1$ materials were close to randomly oriented, while the $40L_1$ materials were strongly oriented. Further, the degree of orientation was about the same in each layer, although the direction was opposite. Although the 40 wt % short and long fibre materials of the first set had roughly the same degree of orientation this was not the case for the second set of short fibre/PP systems. All of them exhibited higher degrees of orientation in both the surface as well as the core regions, when compared to the long fibre composites. For the latter, quite a discrepancy in the orientation factors was detectable especially in the lower filled systems, when using different evaluation methods (Pers. = personal evaluation of scanning electron micrographs; Quant. = measurements by a Quantimet 970 image analyser attached to an optical microscope). Although it can be assumed that the data given by the Quantimet measurement are more accurate because more samples can be evaluated, the average values between both measurements were used here for the long glass fibre (LGF) samples in order to have a comparison with the short glass fibre (SGF) materials which were only evaluated by hand.

Fig. 9 compares the fibre length distributions in the long and short fibre composites using the example of materials $40L_1$ and $40S_1$. It can be seen that the fibres in the pultrusion compounded structure were, in fact, considerably longer than those found in the extruded material. In the latter, the longest fibres were a little over 1 mm long, while the longest fibre in the long fibre material was 10 mm. The slight rise in fibre frequency near 10 mm is not an experimental artefact. In the long fibre materials, the fibre pellets are cut so that they contain fibres which are 10 mm in length, and some of these apparently survived in the injection and mould-filling process unbroken. Also, a strong variation in fibre length distribution through the thickness was not found for these polypropylene matrix materials, in contrast to the polyamide system tested in a previous study [2]. In the polyamide matrix material, the average fibre length in the core regions was found to be nearly twice that found in the surface regions. It was suggested that the increase in fibre degradation was due to the high shear forces which occur in the surface regions during the mould-filling process. Table II shows for two of the long fibre/polypropylene matrix composites that the average fibre length in the surface

TABLE I Microstructural details of the two sets fibre-reinforced PP versions

	Material code	Nominal fibre volume fraction (%)	Overall fibre volume fraction* (%)	Relative core thickness† (C/B)	Core fibre volume fraction* (%)	Surface fibre volume fraction* (%)
Set 1	$10L_1$	3.87	3.9	0.132	4.7	3.8
	$20L_1$	8.30	10.9	0.147	16.5	9.9
	$30L_1$	13.43	14.5	0.223	19.2	13.2
	$40L_1$	19.44	21.3	0.208	31.7	18.6
	$40S_1$	19.44	21.8	0.145	27.4	20.9
Set 2	$10S_2$	3.87	3.8	0.031	4.1	3.7
	$20S_2$	8.30	8.7	0.071	10.2	8.6
	$30S_2$	13.43	13.4	0.086	15.4	13.3
	$40S_2$	19.44	19.5	0.108	21.6	19.2

*From density measurements.
† $C/B + 2S/B = 1$.

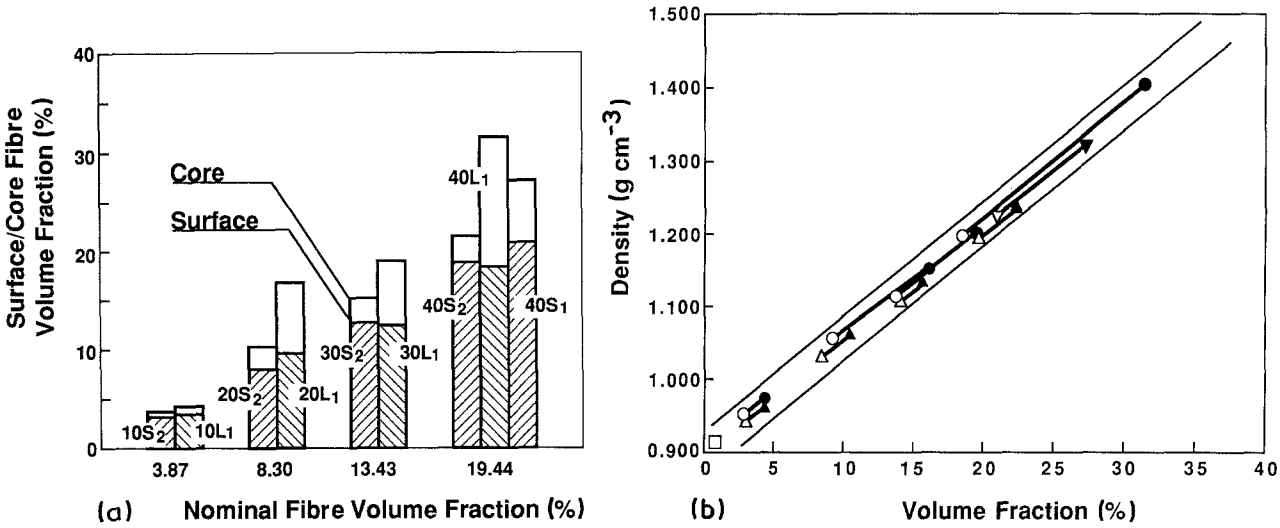

Figure 7 (a) Differences between surface- and core-fibre volume fraction as function of nominal fibre loading in LGF-PP and SGF-PP. (b) Correlation between density and fibre content in the different GF-PP composites. (□) Matrix, (○, ▽, △) surface, (●, ▼, ▲) core, for (○, ●) L_1, (▽, ▼) S_1, (△, ▲) S_2.

region is slightly longer than that in the core region. This is a little puzzling, if shear forces at the wall are responsible for the changes in fibre length distribution. It should perhaps be expected that the difference in fibre degradation should be smaller in the polypropylene material, because it is much more viscoelastic than the polyamide matrix and can be expected to have a blunter velocity profile during the mould-filling process. However, one would expect the higher shear near the walls to cause some increase in the fibre degradation of the surface layers.

Fig. 10 illustrates the fibre length distributions in the second set of short fibre-filled polypropylene samples. It is obvious that the average fibre length is reduced and the distribution becomes narrower the more fibres are incorporated in the polymer matrix. This is in quite good agreement with results found for other polymer matrix systems having a similar kind of reinforcement [5, 12, 13]. The reduction in the overall average fibre length with V_f, also seen for the "longer" fibre-loaded materials, is a consequence of enhanced interaction between the fibres during the mould-filling process with a greater possibility of fibre breakage events (Fig. 11).

One other important feature of the microstructure is shown in Fig. 12. In this photograph of the x–y plane of the $40L_1$ material, large fibre bundles can be seen. These fibre bundles are very common in the $40L_1$ long fibre material and somewhat less common in the $30L_1$ material. Almost no fibre bundles were observed in materials with lower fibre loadings. The short fibre material ($40S_1$) also showed some fibre bundling, though not as much as is visible in Fig. 12. Within the bundles shown in Fig. 12 the fibres tend to be more highly oriented than the individual fibres between them. When the fibre orientation values were calculated, each fibre in a fibre bundle was counted separately. While this is, strictly speaking, correct, it may be that this procedure overestimates the effective orientation of the fibres, because a bundle of n fibres may contribute less to the toughness than an individual fibre. With this in mind, it is possible that the orientation values given in Fig. 8 slightly overestimate the effective orientation of the filler, especially in the case of the $30L_1$ and $40L_1$ materials.

4.2. Mechanical behaviour

4.2.1. Tensile test data

As expected from the literature about the tensile properties of thermoplastics as a function of short fibre

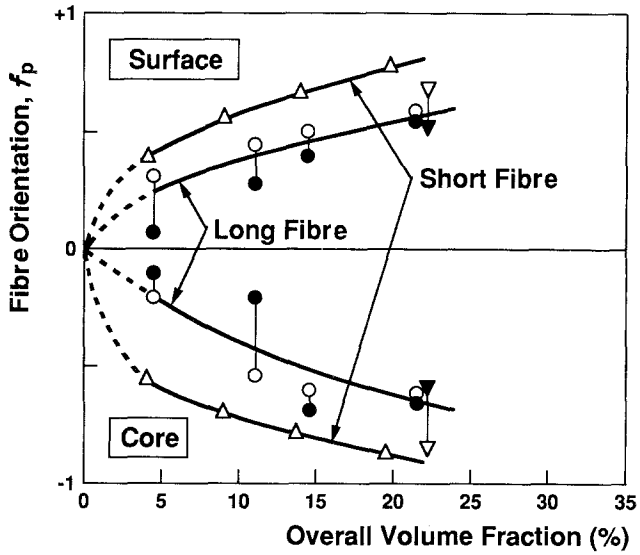

Figure 8 Fibre orientation factors (f_p) in the surface and core regions of the different GF-PP materials. For the LGF-PP, the f_p values were determined by two different methods (Pers. and Quant., see text). (○, ●) L_1, (▽, ▼) S_1, (△) S_2, for (○, ▽, △) Pers., (●, ▼) Quant.

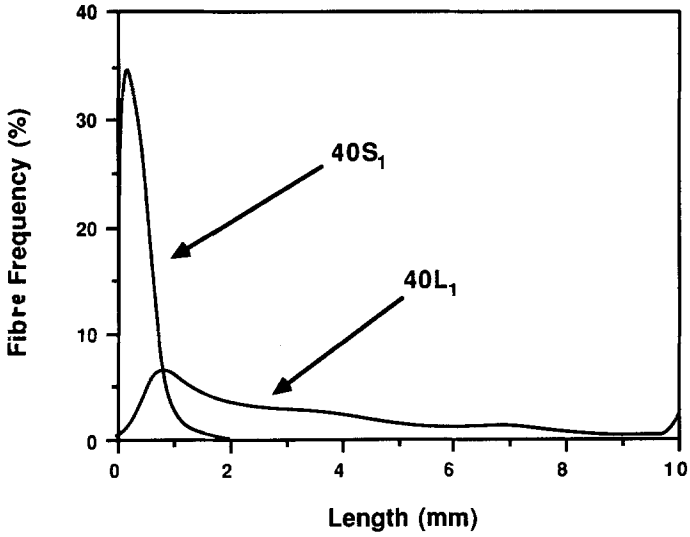

Figure 9 Comparison of fibre length distribution in the surface regions of the $40L_1$ and $40S_1$ materials.

reinforcements, e.g. [14], the fracture strength, σ_f, increases and the strain to failure decreases the more fibres are incorporated (Figs 13a, b). The increase in strength is the most pronounced for specimens with a high amount of fibres parallel to the loading direction (T-specimens) and with longer fibre reinforcement (LGF). An opposite trend holds for the elongation to break (ε_B). It is further seen in Figs 13a and b, that the two sets of 40 wt % short glass fibre-reinforced PP ($40S_1$ and $40S_2$, both processed at different dates and under slightly different conditions) possess the same level of strength and strain to failure. It should be noted here that the ε_B values were calculated from cross-head displacements (without strain gauges) and are therefore somewhat too high. The trends are, however, quite correct.

With respect to the tensile modulus (E_t) it can be noted that the same statements made about the fracture strength are valid: an increase in E_t with (a) increasing fibre content, (b) longer fibre aspect ratio, and (c) a higher amount of fibres parallel to the loading direction (T-specimens). The highest value measured was 10.6 GPa, valid for the T-specimen of material $40L_1$.

4.2.2. Static fracture toughness

The static fracture toughness (K_c) data generated with compact tension specimens at room temperature and a rather low cross-head speed are plotted in Figs 14a and b as a function of nominal fibre volume fraction V_f for the L- and T-crack directions respectively. In both cases, K_c data increase with fibre loading. The absolute values are higher for the specimens with long fibre reinforcement and for those with the crack direction transverse to the fibre orientation in the surface layers (T-crack direction). Further it can be noted that the two different sets of 40 wt % short fibre/PP versions in both directions resulted in almost the same fracture toughness. It seems that the long fibre-filled material with cracks in the T-direction has reached an optimum level of toughness between 30 and 40 wt % fibres (corresponding to 14% to 20% nominal volume fraction). This is quite a common trend also observed with other thermoplastic matrix systems (e.g. [15, 16]) as a result of too high a degree of fibre bundling and a lack of matrix necessary to provide strong enough stress transfer between the fibres.

Fig. 15 illustrates that a rise in testing temperature from 20 to 70° C does not affect the trend and the absolute values of fracture toughness (K_c) enormously. Only a slight drop of the K_c data, but still with an overlap of the scatter bars derived from testing three different samples at each condition, was detectable at the higher temperature level. This reduction is primarily due to a weakening in strength of the polymer matrix material.

TABLE II Average fibre length in the surface and core regions of materials $20L_1$, $40L_1$ and $40S_1$

Material code	Average fibre length (mm)			
	Surface		Core	
	X_n	X_v	X_n	X_v
$20L_1$	4.4	6.3	3.0	4.0
$40L_1$	3.5	5.6	2.8	4.9
$40S_1$	0.47	0.64	0.47	0.64

4.2.3. Notched Izod impact

The results achieved with razor-notched Izod impact specimens can be analysed from different viewpoints. Using the maximum force as a criterion for the resistance of the materials against crack propagation and fracture may lead to a dynamic fracture toughness

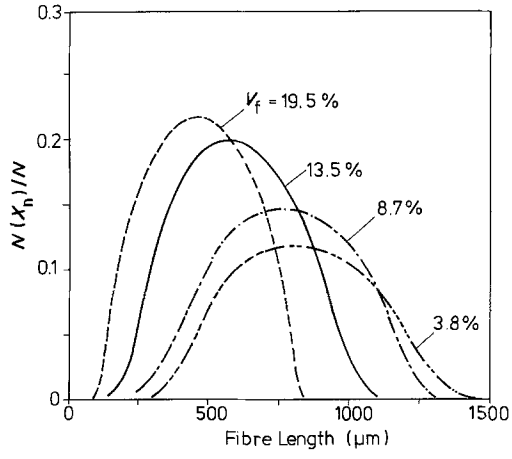

Figure 10 Fibre length distribution in the different short fibre-reinforced PP versions.

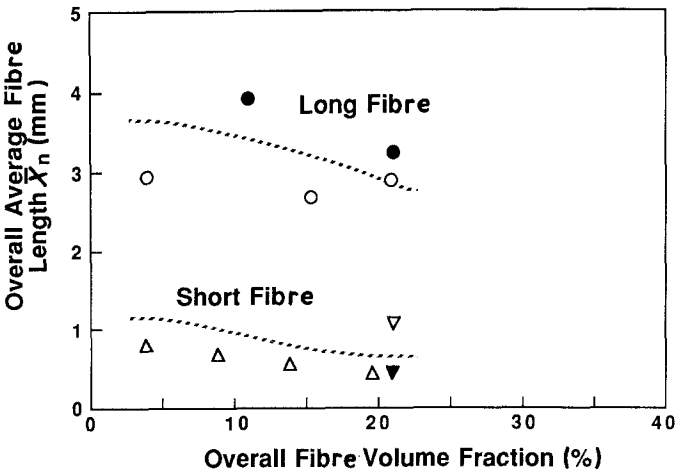

Figure 11 Change in the overall average fibre length with overall fibre volume fraction in LGF-PP and SGF-PP. As the data were determined by two different methods, i.e. a rough measurement of matrix burned-off samples with (○, ▽, △) a light optical microscope (LM) and (●, ▼) a more precise procedure using sieves (SV), the wide scatter is not surprising. (○, ●) L_1, (▽, ▼) S_1, (△) S_2.

value according to the relationship

$$K_d = \frac{F_{max}}{BW} a^{1/2} Y \quad (5)$$

where $Y \approx 23.55$ as a geometrical correction factor, estimated from results of previous studies [17] for Izod impact specimens of the same geometry and crack length. A plot of K_d against the nominal fibre volume fraction should lead to a similar trend found for static fracture toughness (K_c) except that the effect of the higher loading rate will shift the data of these rigid materials to a higher toughness level (Figs 16a, b).

Concerning the absorption of energy up to the point of fracture initiation (E_{peak}), Fig. 17 illustrates that the same trend as seen for the maximum force was, in principle, achieved. Using these values for a calculation of the dynamic fracture toughness, via Equation 6

$$K_d = \left(\frac{E_{peak} E_t}{A} \right)^{1/2} \quad (6)$$

where E_t is the tensile modulus of the different materials and A the cross-section to be fractured, leads for materials $40L_1$ and $40S_1$ to the results given in Table III. Specimens with cracks in the T-direction exhibited higher values than those with L-cracks, and the long fibre-filled material was superior to the short fibre composite. In addition, Table III illustrates that the K_d data calculated from F_{peak} are in quite a good agreement with those generated from the peak energy values.

4.2.4. Instrumented falling weight impact

Figs 18 and 19 show the fracture energies and peak forces measured for the different materials in the falling weight impact tests. The results of these tests are qualitatively similar to those found in Figs 14, 16 and 17, especially because, in both curves, the forces and energies reached a maximum or levelled out between 30 and 40 wt % (15 to 20 vol %) fibre content. The performance of the short fibre materials was considerably worse in these tests. In particular, the $40S_1$ material had a lower fracture energy than the $10L_1$ material.

In Figs 18 and 19 it can also be seen that the fracture energies and the peak forces found in the falling weight test were considerably higher than those found in the Izod tests. Some of these differences can be attributed to differences in the specimen geometry and to different failure modes in the two tests. However, a great deal is due to the fact that the falling weight tests include crack initiation as part of the measured forces and energies, whereas the Izod test does not. This effect has been seen before in tests on similar materials [18].

4.3. Fractography

Fig. 20 shows the fracture surface of a CT-specimen of the unfilled polypropylene homopolymer. Fracture has developed from the initial razor notch by the formation of a few minor crazes and one dominant craze. The latter was followed by some amount of stable crack growth which extended through the specimen over a distance of about 2 mm before crack instability and final fracture took place. In the centre of the specimen the craze and subcritical crack had propagated further ahead than at the edges of the crack front, an indication for the more critical

TABLE III Influence of crack direction and fibre length in GF-PP on the dynamic fracture toughness K_d, as determined from peak forces or fracture energies measured in instrumented Izod tests. The elastic moduli used for calculation are: T direction, $40L_1$ (10.5 GPa), $40S_1$ (10.0 GPa); L direction, $40L_1$ (9.0 GPa), $40S_1$ (6.8 GPa); (cross-section to be fractured: $A = 36.93\,mm^2$)

Material code	Crack direction	Peak force, F_{max} (N)	Fracture toughness,* K_d (MPa $m^{1/2}$)	Fracture energy, E_{peak} (J)	Fracture toughness,† K_d (MPa $m^{1/2}$)
$40L_1$	T	502	9.7	0.373	10.3
	L	410	8.0	0.308	8.7
$40S_1$	T	400	7.8	0.205	7.5
	L	232	1.73	0.082	1.88

*As calculated from F_{max}.
†As calculated from E_{peak}.

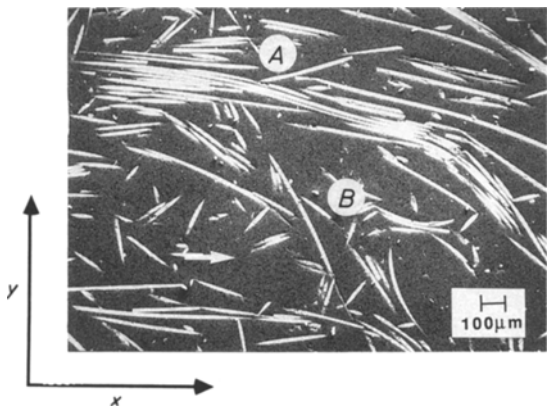

Figure 12 x–y plane of the $40L_1$ material showing a large fibre bundle at point A (the arrow indicates the mould-filling direction) and some bent fibres at the lower right of point B.

three-dimensional stress state in the interior of the material. The surface morphology of the stable part of crack growth is characterized by numerous dimples surrounded by stretched matrix tips (Fig. 21a). The latter can be assumed to be a result of ruptured fibrils in the precrazed material, formed during the transition from craze into crack. Fig. 21b reflects, to the contrary, the fine structure in the region of the crack instability. Here the matrix had failed in the typical brittle manner.

The fracture surfaces of the long fibre-reinforced PP-samples are dominated by numerous fibres and fibre bundles which were pulled-out from the counter-surface. In addition, many holes are visible which resulted from bundles that remained attached to the other half of the broken specimen (Fig. 22). A closer look at the fracture surface, especially in the region where fibres were preferably longitudinally oriented to the crack direction implied that the fibre/matrix bonding was quite poor in this material. The remaining fibres and the fibre imprints were very clean (Fig. 23).

Fig. 24 compares the failure patterns of falling weight impact specimens. The unfilled PP matrix material failed by having a large, almost circular plug punched out of its centre (Fig. 24a). The resulting hole diameter was almost twice that of the striker. Along the edges of the hole, the PP was broken in a totally brittle manner. Short fibre reinforcement of 40 wt % changed the shape of the hole to an oval, with the length axis in orientation of the mould-filling direction (Fig. 24b). The ratio of length to width of the oval hole was about 1.54. This is of the same order of magnitude as the T to L ratios of the K_c or K_d data determined for the $40S_1$ and $40S_2$ materials in the static fracture toughness and notched Izod impact tests (cf. Fig. 14 and Table III: K_{c_T}/K_{c_L} = 1.57 to 1.88). Fig. 24c illustrates that in case of the 40 wt % "long" fibre composite ($40L_1$) the punched holes in the plaques are much more circular, indicating a greater isotropy of this material in comparison to the short fibre version (which is in agreement with the much smaller differences in the K values measured in the T and L direction). In many of these cases pieces of material around the punched hole still remained attached to the specimen surface (Fig. 24d). This can be considered direct evidence that the longer fibres tend to hold the material together much better, therefore giving it much more impact resistance, especially when being loaded in the direction of the plaque thickness B (z direction). Here they also seem to make it much more difficult for cracks to be formed at the moment of the impact of the plaques by the metallic striker. Clear evidence for this fact was recently found by Bailey *et al.* [19], who could distinguish much higher initiation and fracture energy values during instrumented falling weight impact studies for longer compared to shorter fibre-filled polyamide 6.6 composites. They also strengthened the statement that long fibre reinforcements give significant advantages over short fibre ones in the case of impact loading. In fact, relating our fracture energy values (average of L and T directions) of the static fracture toughness tests of the $40L_1$ to that of the $40S_1$ material leads to a factor of about 1.34 (after converting K_c values and the modulus data given in Table III into G_c values via $G_c = K_c^2/E$). The ratio of the average fracture energies in the Izod impact tests could be calculated, on the other hand, as 2.37, and that of the instrumented falling weight impact as 2.24. These higher ratios in the impact test mean a much better effectiveness of the longer fibres under such loading conditions.

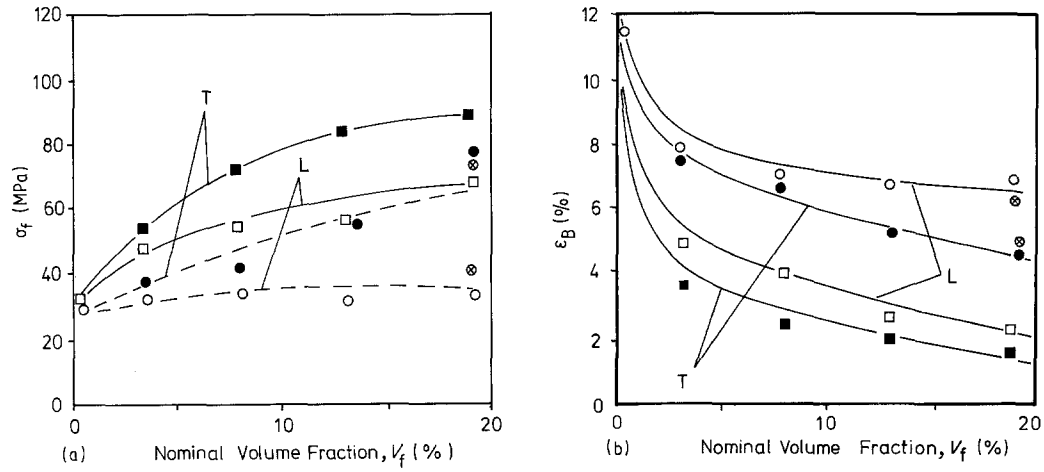

Figure 13 (a) Tensile strength (σ_f) plotted against nominal fibre volume fraction (V_f) of (●, ○) SGF-PP and (■, □) LGF-PP. (⊗) Material $40S_1$. (b) Strain to failure (ε_B) as a function of V_f. For key, see (a).

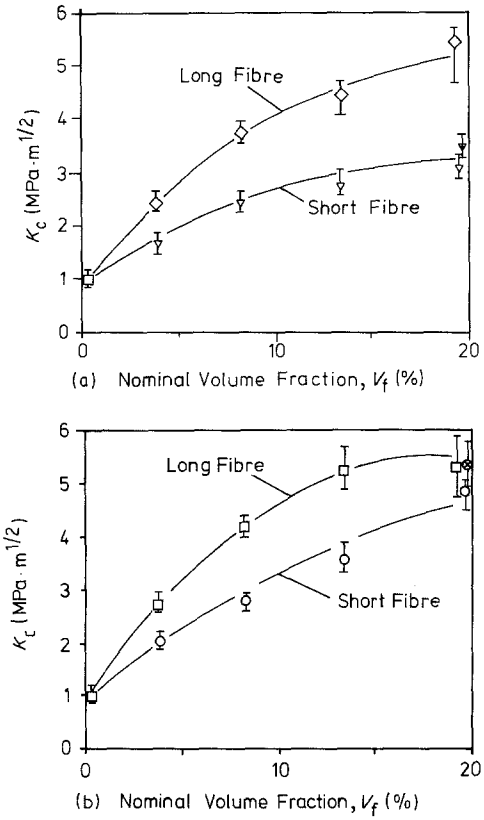

Figure 14 K_c fracture toughness plotted against V_f for the GF-PP composites at room temperature: (a) L direction, (b) T direction (symbols with a cross refer to material $40S_1$).

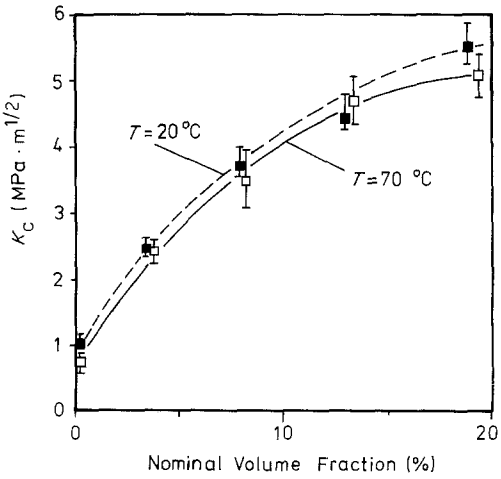

Figure 15 Effect of elevated testing temperature on the course of the K_c–V_f relationship.

4.4. Microstructural efficiency and fracture toughness correlations

A direct comparison between the long and short fibre materials on the basis of the fibre volume fraction is only useful as a first-order approximation, because fibre length aside, they have different microstructures (among other things, the short fibre materials have much thinner cores than the long fibre materials). Because of this deficiency Friedrich [4] has successfully developed a semi-empirical microstructure–toughness

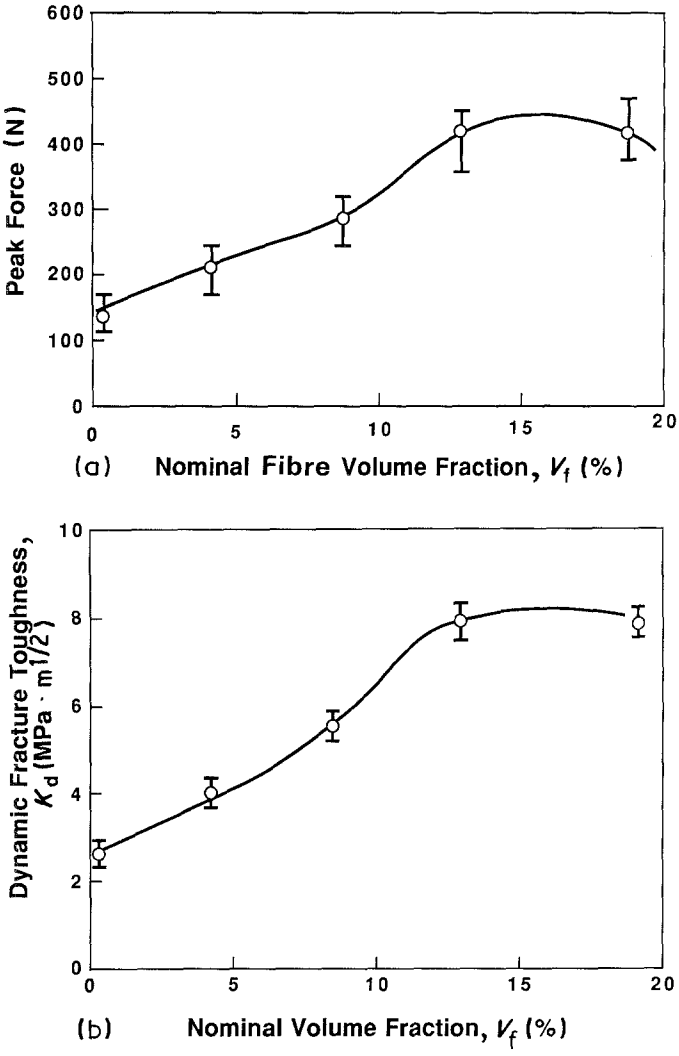

Figure 16 (a) Maximum force plotted against fibre volume fraction of LGF-PP samples, tested under Izod impact loading with notches in the L-direction. (b) Corresponding dynamic fracture toughness values of LGF-PP composites.

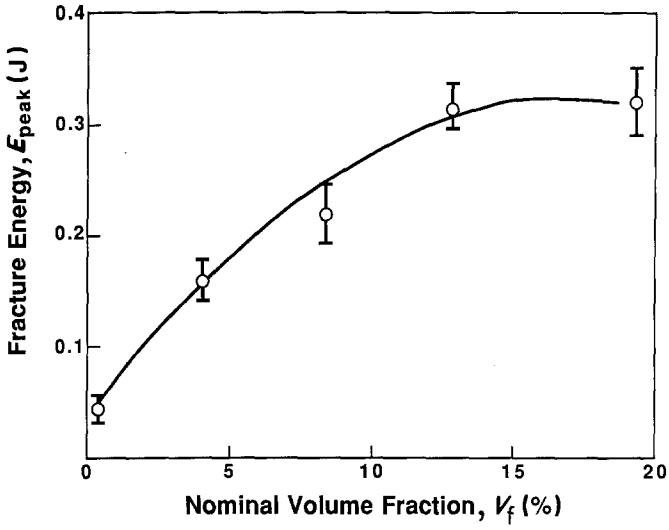

Figure 17 Izod impact fracture energy plotted against V_f for the GF-PP composites at room temperature.

correlation, which accounts for differences in fibre-related microstructural details. This correlation takes the form

$$K_{c,C} = MK_{c,M} \quad (7)$$

where $K_{c,C}$ is the fracture toughness of the composite, M is a microstructural efficiency factor and $K_{c,M}$ is the toughness of the matrix. M is assumed to be the sum of a matrix toughness correction factor a^*, and a mainly fibre-dependent contribution nR, i.e.

$$M = a^* + nR \quad (8)$$

In this equation, a^* takes into account the fact that the matrix may not fail in the same way in the composite as when being tested separately. If it does, the value of a^* should be 1. In general, it can be expected for brittle matrices that a^* will be greater than 1, while for ductile matrices a^* may be less than 1. In Equation 8, n is essentially a scaling factor which should remain constant as long as the temperature, testing conditions and composite system remain constant. If, however, changes in the components of the composite system take place, e.g. other fibre/matrix bond quality, other fibre material or changes in the fibre aspect ratio, this should also result in different values of the "energy absorption ratio" n. R is a reinforcement effectiveness parameter which takes into account the geometrical features of the composite microstructure and has the form [3]

$$R = f_{pe,S} V_{f,S} \frac{2S}{B} + f_{pe,C} V_{f,C} \frac{C}{B} \quad (9)$$

where $V_{f,S}$ and $V_{f,C}$ are the volume fraction of fibres in the surface and the core region, respectively, S is the thickness of the surface region, C is the thickness of the core region, and B is the total thickness of the

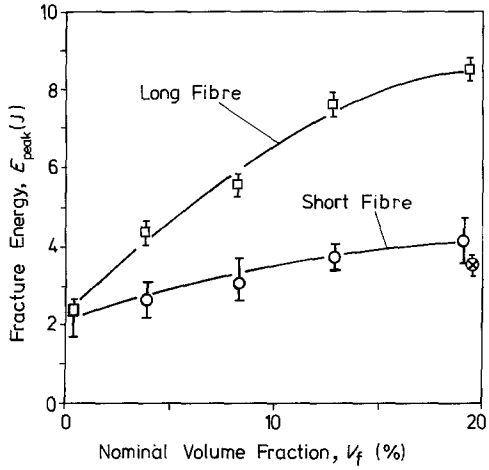

Figure 18 Falling weight impact fracture energy plotted against V_f for GF-PP composites at room temperature.

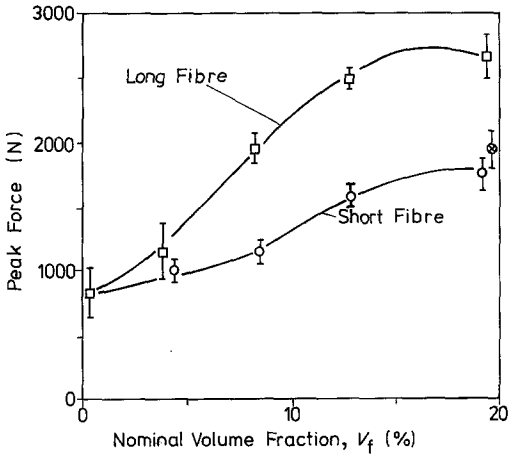

Figure 19 Peak force in the falling weight impact test as a function of nominal fibre volume fraction for SGF-PP and LGF-PP.

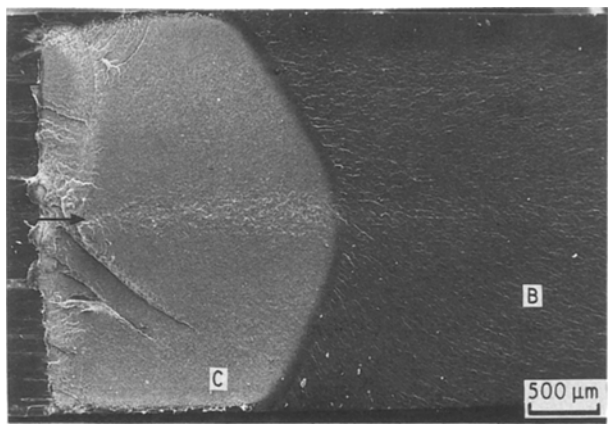

Figure 20 Scanning electron micrograph of the CT-fracture surface of unfilled PP. (C = crazed region; B = unstable, brittle fracture; arrow = beginning and direction of craze and crack growth immediately after the initial razor notch.)

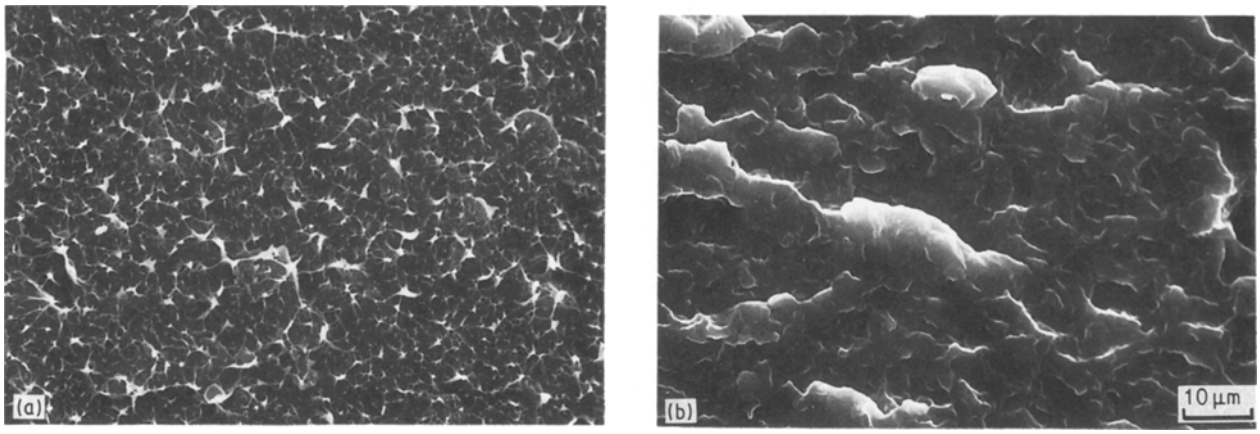

Figure 21 (a) Higher magnification of the crazed region shown in Fig. 20. (b) Magnification of region B in Fig. 20.

sample. The parameters $f_{pe,S}$ and $f_{pe,C}$ are the effective orientation factors for the surface and core layers, respectively. These are approximated using the relation

$$f_{pe} \approx \alpha[1 + \tanh(\beta f_p)] \quad (10)$$

where $\alpha = 0.5$ and $1 < \beta < 5$ [4]. Note that when f_{pe} is calculated for a T direction test, the reference direction in Equation 2 is the mould-filling direction and when f_{pe} is calculated for an L direction test, the reference direction is the y direction perpendicular to the mould-filling direction. If Equations 7 to 10 are valid, a plot of $K_{c,C}/K_{c,M}$ against R should produce a straight line whose intercept is near 1. Values of R for all the materials and test directions are shown in Table IV.

Fig. 25 shows a plot of $K_{c,C}/K_{c,M}$ against R for all the data already mentioned in connection with Figs 14a and b. It can be seen that almost all the data of the LGF and SGF samples each fall on reasonably straight lines whose intercept with the ordinate axis is at about 1.75. As expected, the slope of the short fibre composites is clearly flatter than that for the long fibre-filled PP-materials. This means, at a given value of the reinforcing effectiveness parameter, R, longer fibres result in higher improvements of the polymer's fracture toughness than do shorter ones. The relative increase is, however, not as pronounced as one could expect from the differences in the average fibre length. This is mainly due to the greater degree of fibre bundling in the LGF-materials. To account for these effects, the relatively simple correlation outlined above was modified quite recently by Karger–Kocsis and Friedrich [2], but will not be further discussed in context with the results of this study.

5. Conclusions

In conclusion, it can be stated that the addition of longer fibres to a polypropylene matrix does improve the fracture toughness of the composite over shorter fibre-filled composites, although the magnitude of the increase is highly test dependent. In particular, the long fibre material performed better when energy-related fracture toughnesses were considered (impact tests) than when the strength-related K_c toughness was considered. This is also seen when the impact fracture strengths are compared to the impact fracture energies. The longer fibres contribute more to the ability of the material to absorb energy than they do to its strength.

It was also found that the longer fibre-filled material had a propensity to form fibre bundles, especially at higher loadings, and that this probably caused the effectiveness of the fibre reinforcement to drop off considerably between 30 and 40 wt %.

Additionally, the usefulness of the fracture toughness–microstructure correlation given in

Figure 22 Section of a CT-fracture surface of a 40 wt % LGF-PP specimen showing longitudinally and transversely oriented fibres and fibre bundles (B) as well as holes (H) where complete bundles had been pulled-out.

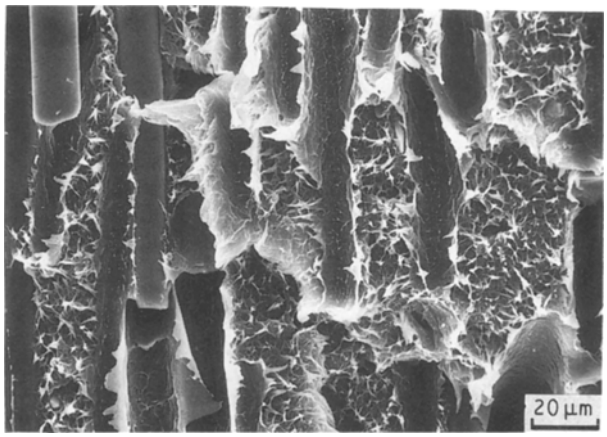

Figure 23 Enlargement of a region in Fig. 22 where fibres were primarily oriented parallel to the fracture surface. Ductile matrix fracture, fibre imprints and poorly bonded fibres are visible.

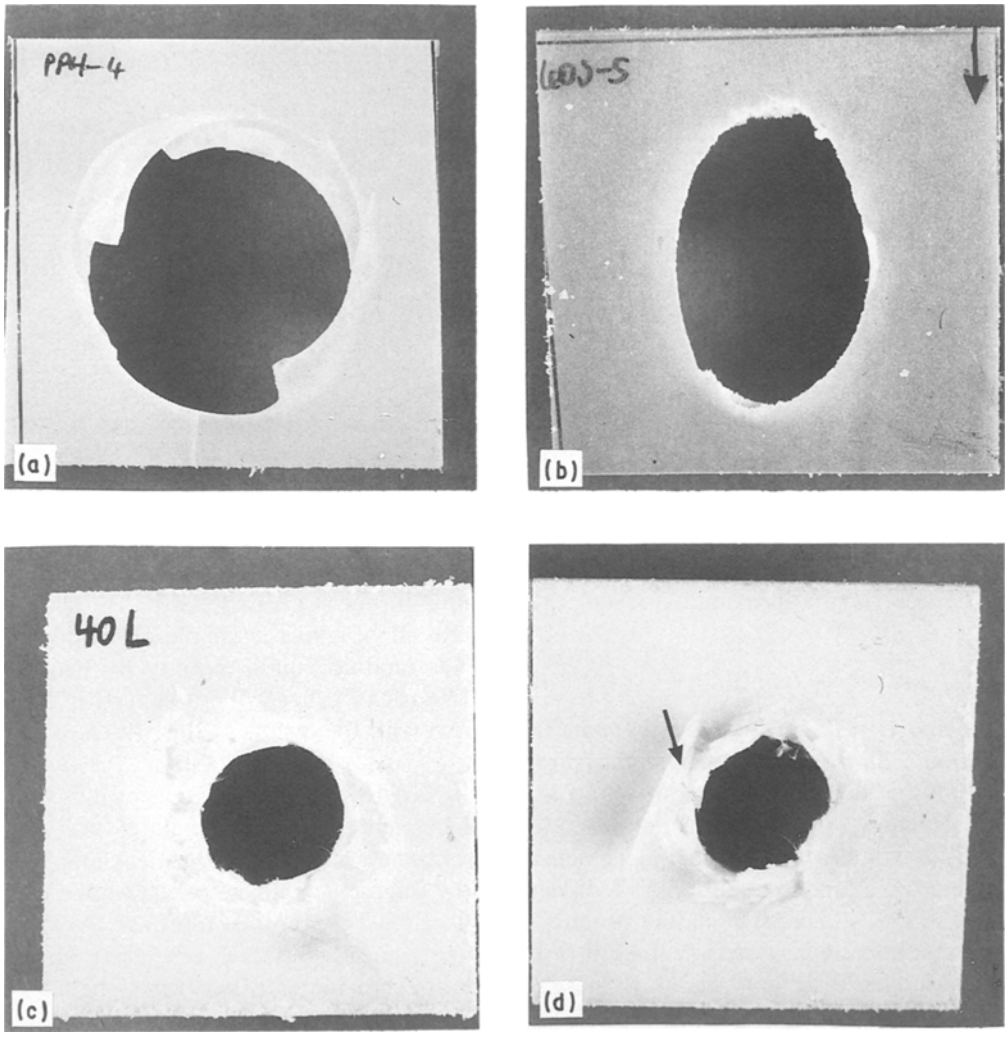

Figure 24 Comparison of falling weight test specimens: (a) neat PP matrix; (b) 40 wt % SGF-PP (arrow indicates mould filling direction); (c) and (d) represent material $40L_1$ with more circular holes and partly with still attached material around the edges (arrow).

Equations 7 to 10 was shown. This correlation predicted the relatively low toughness anisotropy of these materials, and helped to separate the effects of microstructure from the effects of changes in composite system.

Acknowledgements

This paper is dedicated to Professor H. J. Sinn, University of Hamburg, on the occasion of his 60th birthday. The support of this research project by the Deutsche Forschungsgemeinschaft (DFG-FR-675-2-2)

TABLE IV Normalized toughness, effective orientation factors and reinforcing effectiveness factor R for the different GF-PP materials and crack directions. (Note: $f_{p,e\parallel}$ has to be used when the fibres in the layer considered are nearly parallel to the crack, and the opposite is true for $f_{p,e\perp}$)

Material code	Test direction	$\frac{K_{c,C}}{K_{c,M}}$	$f_{p,e\parallel}$		$f_{p,e\perp}$		R
			Surface	Core	Surface	Core	
$10L_1$	L	2.5	0.38	–	–	0.58	0.016
	T	2.7	–	0.42	0.63	–	0.023
$20L_1$	L	3.8	0.31	–	–	0.70	0.043
	T	4.2	–	0.30	0.69	–	0.066
$30L_1$	L	4.5	0.29	–	–	0.78	0.063
	T	5.2	–	0.22	0.71	–	0.082
$40L_1$	L	5.6	0.23	–	–	0.78	0.085
	T	5.3	–	0.22	0.77	–	0.128
$40S_1$	L	3.4	0.22	–	–	0.80	0.071
	T	5.4	–	0.20	0.79	–	0.149
$10S_2$	L	1.6	0.32	–	–	0.75	0.012
	T	2.0	–	0.25	0.68	–	0.025
$20S_2$	L	2.3	0.25	–	–	0.79	0.026
	T	2.8	–	0.22	0.75	–	0.062
$30S_2$	L	2.7	0.22	–	–	0.81	0.037
	T	3.4	–	0.19	0.79	–	0.099
$40S_2$	L	3.1	0.18	–	–	0.85	0.050
	T	4.9	–	0.16	0.82	–	0.144

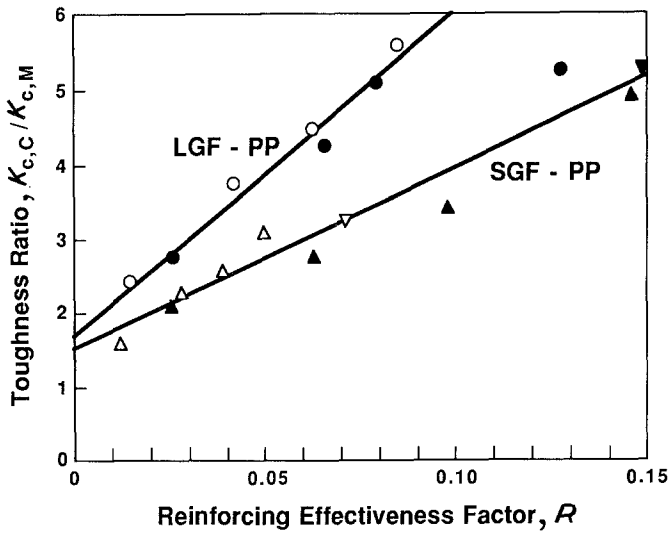

Figure 25 Relative changes in fracture toughness with increasing reinforcing effectiveness factor R for materials SGF-PP and LGF-PP. (○, ▽, △) L, (●, ▼, ▲) T, for (○, ●) $10L_1$ to $40L_1$, (▽, ▼) $40S_1$, (△, ▲) $10S_2$ to $40S_2$.

is gratefully acknowledged. We thank ICI, Wilton, UK, for supplying the testing material and for some financial help to perform this project successfully. Personal thanks should be addressed to G. Nutting, ICI, for material processing, and R. Walter and E. Reese, TUHH, for their invaluable assistance, technical and otherwise, during D. Spahr's stay in Hamburg. K. Friedrich appreciates the help of the Center for Composite Materials, University of Delaware, USA, during the preparation of this paper.

References

1. A. G. GIBSON, A. N. McCLELLAND, G. CUFF and C. R. GORE, "Processing of long fibre reinforced thermoplastics", in "Developments in the Science and Technology of Composite Materials", ECCM-I Conference, 24 to 27 September, 1985, Bordeaux, edited by A. R. Bunsell, P. Lamicq and A. Massiah, pp. 511–19.
2. J. KARGER-KOCSIS and K. FRIEDRICH, *Compos. Sci. Technol.* **32** (1988) 293.
3. *Idem, Composites* **19** (1988) 105.
4. K. FRIEDRICH, *Compos. Sci. Technol.* **22** (1985) 43.
5. K. FRIEDRICH, R. WALTER, H. VOSS and J. KARGER-KOCSIS, *Composites* **17** (1986) 205.
6. J. C. MALZAHN and J. M. SCHULTZ, *Compos. Sci. Technol.* **25** (1986) 187.
7. M. W. DARLINGTON, P. L. McGINLEY and G. R. SMITH, *J. Mater. Sci.* **11** (1976) 877.
8. P. F. BRIGHT, R. J. CROWSON and M. J. FOLKES, *ibid.* **13** (1978) 2497.
9. P. F. BRIGHT and M. W. DARLINGTON, *Plast. Rubb. Process. Appl.* **1** (1981) 139.
10. J. R. VINSON and R. L. SIERAKOWSKI, "The Behavior of Structures Composed of Composite Materials" (Martinus Nijhoff, Boston, 1986) p. 297.
11. D. BROEK, "Elementary Engineering Fracture Mechanics", 3rd Edn (Martinus Nijhoff, The Hague, 1984) p. 76.
12. H. VOSS and K. FRIEDRICH, *J. Mater. Sci.* **21** (1986) 2889.
13. H. VOSS, "Aufbau, Bruchverhalten und Verschleißeigenschaften Kurzfaserverstärkter Hochleistungsthermoplaste", VDI Fortschr. Ber., Reihe 5, No. 116 (VDI Verlag, Düsseldorf, 1987).
14. M. J. FOLKES, "Short Fibre-Reinforced Thermoplastics" (Research Studies Press, Chichester, 1982).
15. K. FRIEDRICH, *Plast. Rubb. Process. Appl.* **3** (1983) 255.
16. F. RAMSTEINER and R. THEYSOHN, *Composites* **10** (1979) 111.
17. K. FRIEDRICH, R. WALTER and J. VOIGT, *J. Thermoplastics Compos. Mater.* **1** (1988) 68.
18. E. M. SILVERMAN, *Polym. Compos.* **8** (1987) 8.
19. R. S. BAILEY, M. DAVIES and D. R. MOORE, unpublished (1989).

Received 19 April
and accepted 20 June 1989